Available online at www.sciencedirect.com
ScienceDirect
Journal of Power Sources 179 (2008) 240–251
JOURNAL OF POWER SOURCES
www.elsevier.com/locate/jpowsour

Effect of anisotropic thermal conductivity of the GDL and current collector rib width on two-phase transport in a PEM fuel cell

Chaitanya J. Bapat, Stefan T. Thynell *

Department of Mechanical and Nuclear Engineering, The Pennsylvania State University, University Park, PA 16802, United States

Received 4 November 2007; received in revised form 9 December 2007; accepted 10 December 2007
Available online 23 December 2007

Abstract

A two-dimensional two-phase model based on the classical two-fluid model is used to analyze electrochemical and thermal transport in a PEMFC. The model is extended to account for the dependence of interfacial area density on liquid volume fraction. At a given fixed voltage, the fuel cell generates maximum current density for low through-plane and high in-plane thermal conductivities at high humidity operating conditions. It is also predicted that for low humidity operating conditions, the fuel cell generates maximum current density if the GDL is tailored to have high through-plane thermal conductivity near the inlet and progressively decreasing through-plane thermal conductivity at distances away from the inlet. At fully humidified cathode inlet conditions, narrower current collector ribs generate higher current densities at all voltages by reducing the resistance to diffusion of reactants and products through the GDL. In order to maximize the current density at low humidities, ribs must be wider near the inlet and narrower away from the inlet. The proposed methodology for tailoring GDL through-plane thermal conductivities and rib widths reduces the risk of membrane dehydration near inlet and also reduces the possibility of excessive liquid accumulation in the region away form the inlet.

Keywords: PEM fuel cell; Two-phase flow; Anisotropy; Thermal conductivity; Rib width; Low humidity operation

1. Introduction

Over the past few years, there has been an increasing interest in the use of proton exchange membrane (PEM) fuel cells (FCs) as an environmentally friendly power source. In these cells, oxygen and hydrogen combine to form water, and a part of the released energy from the reaction is directly converted to electricity.

Liquid water is produced in the cathode catalyst layer due to electrochemical reactions. Excessive amount of liquid water in the cathode GDL reduces the flow of reactants to the catalyst layer by clogging the GDL pores. It also reduces the reaction rate by covering the reaction sites [1]. The amount of liquid water accumulated in the cathode GDL depends on many factors, including the temperature distribution inside the cell as it controls the phase change of water. Over the past few years many different models have been developed to analyze the water and heat management problems in a fuel cell. The earliest models [2–6] did not include an explicit two-phase model to account for the liquid water transport in the catalyst layers and GDLs. Thus, these single-phase models were unable to accurately predict the polarization behavior at high current densities where the effects of liquid water accumulation are most severe [7]. Hence, different two-phase models were developed [7–20] to account for the effect of liquid water transport. The two-phase models were based on the unsaturated flow theory [21] or the multiphase mixture model [22]. Meng [23] and Weber and Newman [24,25] further developed improved models for water transport in the ionic membrane. The effects of various flow and transport properties on the polarization behavior were analyzed using these single-phase and two-phase models.

The effect of the thermal conductivity of the GDLs on polarization behavior was analyzed by Ju et al. [26] using a single-phase model. The authors also assumed the GDL thermal conductivity to be isotropic. The GDLs are commonly constructed of carbon fibers either in woven or paper form. Electron micrographs for different GDLs [27] suggest that the carbon

* Corresponding author. Tel.: +1 814 865 1345.
E-mail addresses: cjb282@psu.edu (C.J. Bapat), Thynell@psu.edu (S.T. Thynell).

0378-7753/$ – see front matter © 2008 Elsevier B.V. All rights reserved.
doi:10.1016/j.jpowsour.2007.12.033

Nomenclature

a	water vapor activity
A	active area (m^2)
A_{cross}	area of cross-section of the channel (m^2)
A_{lg}	gas–liquid interfacial area per unit volume (m^{-1})
c	specific heat capacity ($kJ\,kg^{-1}\,K^{-1}$)
C	molar concentration ($mole\,m^{-3}$)
d_{hyd}	hydraulic diameter (m)
D	diffusivity ($m^2\,s^{-1}$)
EW	equivalent weight ($kg\,equiv^{-1}$)
F	Faradays constant ($C\,mole^{-1}$)
GDL	gas diffusion layer
h	convective heat transfer coefficient ($W\,m^{-2}\,K^{-1}$)
$\mathbf{i}$, i	local ionic current density ($A\,m^{-2}$)
i_0^{ref}	reference current density ($A\,m^{-3}$)
i_{tot}	total current density produced by the fuel cell ($A\,m^{-2}$)
j	volumetric electrochemical reaction rate ($A\,m^{-3}$)
$\mathbf{k}$	thermal conductivity ($W\,m^{-1}\,K^{-1}$)
k_f	thermal conductivity of fluid ($W\,m^{-1}\,K^{-1}$)
k_{xx}	through-plane thermal conductivity ($W\,m^{-1}\,K^{-1}$)
k_{yy}	in-plane thermal conductivity ($W\,m^{-1}\,K^{-1}$)
K_{gr}	relative permeability for gas phase
K_H	Henry's law constant ($Pa\,m^3\,mole^{-1}$)
K_{lr}	relative permeability for liquid phase
K_p	hydraulic permeability (m^2)
MEA	membrane electrode assembly
n_{oe}	electro-osmotic drag coefficient
Nu	Nusselt number
p	pressure (Pa)
P	perimeter of cross-section (m)
PEM	proton exchange membrane
R	universal gas constant ($J\,mole^{-1}\,K^{-1}$), electric resistance (Ω)
S	volumetric source term ($mole\,m^{-3}\,s^{-1}$)
t	time (s)
T	temperature (K)
U_o	open circuit potential (V)
$\mathbf{v}$	velocity ($m\,s^{-1}$)
V_0	molar specific volume of water ($m^3\,mole^{-1}$)
V_{cell}	cell voltage (V)
ΔV_{net}	total volume of all the computational cells adjacent to the GDL/bipolar plate interface

Greek letters

α	phase volume fraction
α_a	anodic transfer coefficient
α_c	cathodic transfer coefficient
γ_{lg}	interphase molar transfer coefficient ($m\,s^{-1}$)
ε	porosity
θ	contact angle (°)
κ	membrane ionic conductivity ($S\,m^{-1}$)
μ	viscosity ($Pa\,s$)
ρ	density ($kg\,m^{-3}$)
σ	surface tension ($N\,m^{-1}$), electrical resistivity ($\Omega\,m$)
τ	viscous stress (Pa)
ϕ	potential (V)

Subscripts

a	anode
c	capillary, cathode
eq	equivalent
g	gas
l	liquid
m	membrane
p	constant pressure
por	porous material
wp	wetting phase

Superscripts

i	component

fibers are preferentially oriented in the in-plane direction. The thermal conductivity measurements for polymers with preferential fiber orientation [28–31] and also for certain GDLs [32,33] suggest that the thermal conductivity of the GDLs is highly anisotropic. The effect of anisotropic thermal conductivity on multicomponent transport in a fuel cell cathode was considered by Pasaogullari et al. [34] using the multiphase mixture model [22] and by Pharoah et al. [35] using a single-phase model. In this paper, we extend our previous work [36] to present an analysis of the effect of both the magnitude and anisotropy of the GDL thermal conductivity on polarization characteristics at low and high humidity operating conditions using a two-dimensional two-phase model. We also analyze the effect of current collector rib width on polarization behavior. We use the classical two-fluid model proposed by Ishii [37], Drew and Passman [38] and Hassanizadeh and Gray [39,40] in our work and also account for the effect of electrical and thermal contact resistance at the GDL/bipolar plate interface. In the next section we describe in detail the mathematical model used for our work.

2. Model formulation

The model presented here (see Table 1) accounts for flow of reactants, products and ionic species, as well as the generation and transport of heat. The two-dimensional computational domain used in our work is shown in Fig. 1 along with a schematic for a PEMFC. The assumptions and simplifications used in our model are described next.

2.1. Flow model

We use a two-phase model to analyze transport of species in the catalyst layers and GDLs. As stated in Section 1, the two-

Table 1
Model equations and source terms

Equation	Ref.
Electrochemical reactions:	
$-\nabla\cdot(\kappa\nabla\phi_m) = FS^{H^+}$	
$FS^{H^+} = j_c =$	[41]
$\alpha_g i_{oc}^{ref}\left[\exp\left\{\frac{\alpha_a F}{RT}(\phi_s-\phi_m)\right\}-\exp\left\{-\frac{\alpha_c F}{RT}(\phi_s-\phi_m)\right\}\right]\left(\frac{C_g^{O_2}}{C_{ref}^{O_2}}\right)+\alpha_l i_{oc}^{ref}\left[\exp\left\{\frac{\alpha_a F}{RT}(\phi_s-\phi_m)\right\}-\exp\left\{-\frac{\alpha_c F}{RT}(\phi_s-\phi_m)\right\}\right]\left(\frac{C_l^{O_2}}{C_{ref}^{O_2}}\right)$ at cathode	
$FS^{H^+} = j_a =$	
$\alpha_g i_{oa}^{ref}\left[\exp\left\{\frac{\alpha_a F}{RT}(\phi_s-\phi_m)\right\}-\exp\left\{-\frac{\alpha_c F}{RT}(\phi_s-\phi_m)\right\}\right]\left(\frac{C_g^{H_2}}{C_{ref}^{H_2}}\right)^{\frac{1}{2}}+\alpha_l i_{oa}^{ref}\left[\exp\left\{\frac{\alpha_a F}{RT}(\phi_s-\phi_m)\right\}-\exp\left\{-\frac{\alpha_c F}{RT}(\phi_s-\phi_m)\right\}\right]\left(\frac{C_l^{H_2}}{C_{ref}^{H_2}}\right)^{\frac{1}{2}}$ at anode	
Gas/Liquid phase species transport:	
For $i = O_2, H_2, N_2$	
$\frac{\partial\varepsilon\alpha_{g/l}C_{g/l}^i}{\partial t}+\nabla\cdot(\varepsilon\alpha_{g/l}C_{g/l}^i\mathbf{v}_{g/l}) = \nabla\cdot(\varepsilon\alpha_{g/l}D_{g/l}^i\nabla C_{g/l}^i)\mp\gamma_{lg}^i\left(\frac{RT}{K_H^i}C_g^i-C_l^i\right)A_{lg}+S_{g/l}^i$	[39,40]
In catalyst layers	
$S_{g/l}^{O_2} = \frac{1}{4F}\alpha_{g/l}i_{oc}^{ref}\left[\exp\left\{\frac{\alpha_a F}{RT}(\phi_s-\phi_m)\right\}-\exp\left\{-\frac{\alpha_c F}{RT}(\phi_s-\phi_m)\right\}\right]\left(\frac{C_{g/l}^{O_2}}{C_{ref}^{O_2}}\right)$	
$S_{g/l}^{H_2} = -\frac{1}{2F}\alpha_{g/l}i_{oa}^{ref}\left[\exp\left\{\frac{\alpha_a F}{RT}(\phi_s-\phi_m)\right\}-\exp\left\{-\frac{\alpha_c F}{RT}(\phi_s-\phi_m)\right\}\right]\left(\frac{C_{g/l}^{H_2}}{C_{ref}^{H_2}}\right)^{\frac{1}{2}}$	
and $S_{g/l}^i = 0$ everywhere else. Nitrogen does not take part in chemical reactions.	
Component balance for water:	
In catalyst layers and GDLs	
$\frac{\partial\varepsilon\alpha_{g/l}C_{g/l}^{H_2O}}{\partial t}+\nabla\cdot(\varepsilon\alpha_{g/l}C_{g/l}^{H_2O}\mathbf{v}_{g/l}) = \nabla\cdot(\varepsilon\alpha_{g/l}D_{g/l}^{H_2O}\nabla C_{g/l}^{H_2O})\mp\gamma_{lg}^{H_2O}\left(C_g^{H_2O}-\frac{P_{sat,H_2O}}{RT}\right)A_{lg}+S_{g/l}^{H_2O}$	[39,40]
In membrane	
$\frac{\partial\varepsilon\alpha_g C_g^{H_2O}}{\partial t} = \nabla\cdot(\varepsilon\alpha_g D_g^{H_2O}\nabla C_g^{H_2O})+S_g^{H_2O}$	
$S_g^{H_2O} = -\nabla\cdot\left(\frac{n_{oe}}{F}\mathbf{i}\right)$ in membrane and catalyst layers $S_l^{H_2O} = -\frac{j_c}{2F}$ in cathode catalyst layer	
Two phase momentum balance:	
$\frac{\partial\varepsilon\alpha_{g/l}\rho_{g/l}\mathbf{v}_{g/l}}{\partial t}+\nabla\cdot\varepsilon\alpha_{g/l}\rho_{g/l}\mathbf{v}_{g/l}\mathbf{v}_{g/l} = -\nabla\varepsilon\alpha_{g/l}p_{g/l}+\nabla\cdot\varepsilon\alpha_{g/l}\tau_{g/l}-\frac{\mathbf{v}_{g/l}\mu_{g/l}}{K_p K_{g/lr}}$ and $p_l = p_g - p_c$	[39,40]
Heat balance equation:	
$\frac{\partial}{\partial t}(\rho_{eq}c_{eq}T)+\nabla\cdot(\varepsilon\alpha_l\rho_l\mathbf{v}_l c_l T)+\nabla\cdot(\varepsilon\alpha_g\rho_g\mathbf{v}_g c_{pg}T) = \nabla\cdot(\mathbf{k}_{eq}\cdot\nabla T)+\gamma_{lg}^{H_2O}\left(C_g^{H_2O}-\frac{P_{sat,H_2O}}{RT}\right)A_{lg}M^{H_2O}L_w+q'''$	
$\rho_{eq}c_{eq} = (1-\varepsilon)\rho_{por}c_{por}+\varepsilon\alpha_l\rho_l c_l+\varepsilon\alpha_g\rho_g c_{pg}$	[36]
$\mathbf{k}_{eq} = (1-\varepsilon)\mathbf{k}_{por}+\varepsilon\alpha_l\mathbf{k}_l+\varepsilon\alpha_g\mathbf{k}_g$	
where $q''' = \lvert j_a(\phi_s-\phi_m)\rvert+\frac{i^2}{\kappa}$ in anode catalyst layer $q''' = \frac{i^2}{\kappa}$ in membrane $q''' = \lvert j_c(\phi_s-\phi_m)\rvert+\frac{i^2}{\kappa}+\lvert T\Delta S\frac{j_a}{2F}\rvert$ in cathode catalyst layer $q''' = i_{tot}^2\sigma$ in GDLs $q''' = \frac{(i_{tot}A)^2R_{c,contact}}{\Delta V_{net}}$ for a computational cell adjacent to GDL/bipolar plate interface Also see Table 3 for a simplified expression for $\mathbf{k}_{eq}$.	

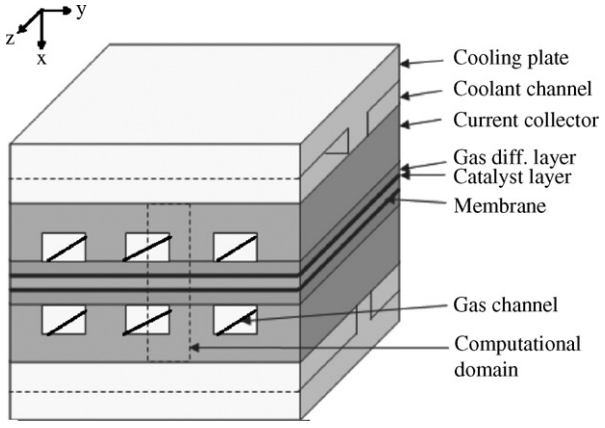

Fig. 1. The computational domain and schematic of a PEM fuel cell.

phase transport of different species is modeled using the classical two-fluid model proposed by Ishii [37], Drew and Passman [38] and Hassanizadeh and Gray [39,40]. The porous drag is modeled using a source term based on the Darcy law. The effects of phase change and species dissolution are modeled using rate expressions which account for the effect of gas-liquid interfacial area density.

We use a single-phase model for transport inside the membrane which means that we do not allow the liquid water produced at cathode to enter the membrane and consider only the concentration-driven diffusion of water vapor through the membrane. We also do not consider phase change of water inside the membrane. The assumption of single-phase transport inside the ionic membrane seems reasonable for two reasons: the hydraulic permeability of the membrane is a few orders of magnitude lower than the hydraulic permeability of the GDL (see Table 2) and the membrane is known to be at least slightly hydrophobic with pore radii much smaller than the GDL [24,25]. The overall effect of

Table 2
Model parameters and properties

Quantity	Value
Gas channel length (m)	1.577 [54]
Gas channel width (m)	2.16E−3 [54]
Current collector width (m)	0.89E−3 [54]
Active area (m^2)	50E−4 [54]
Membrane	Nafion® 112 [54]
Gas-diffusion layer thickness (m)	350E−6 [48]
Catalyst layer thickness (m)	10.0E−6
Height of the symmetrical section (m)	1.525E−3
Anode humidification temperature (K)	353 [54]
Cathode humidification temperature (K)	353 [54]
Anode inlet stoichiometry ($A\,m^{-2}$ equiv)	1.875E4 [54]
Cathode inlet stoichiometry ($A\,m^{-2}$ equiv)	1.125E4 [54]
Coolant water temperature (K)	353 (assumed)
Cathode inlet pressure (atm)	1.5 [54]
Anode inlet pressure (atm)	1.5 [54]
Gas-diffusion layer electrical resistivity ($\Omega\,m$)	80.0E−5 [32]
Through-plane thermal conductivity of gas-diffusion layers k_{xx} ($W\,m^{-1}\,K^{-1}$)	0.22 [49]
Ratio of thermal conductivities k_{yy}/k_{xx}	20:1 (assumed based on [32])
Thermal conductivity of the membrane ($W\,m^{-1}\,K^{-1}$)	0.16 [49]
Thermal conductivity of the catalyst layer ($W\,m^{-1}\,K^{-1}$)	0.27 [49]
Thermal conductivity of current collector, steel ($W\,m^{-1}\,K^{-1}$)	16.0
GDL/Bipolar plate thermal contact conductance ($W\,m^{-2}\,K^{-1}$)	10,000 (assumed based on [61])
GDL/Bipolar plate electrical contact resistance ($m\Omega\,cm^2$)	41.7 [54]
Gas-diffusion layer porosity	0.74 [27]
Maximum interfacial area density (m^{-1})	500
Catalyst layer porosity	0.15 (fitted)
Hydraulic permeability of GDL (m^2)	6.3E−12 [48]
Hydraulic permeability of membrane (m^2)	1.0E−18 [25]
Hydraulic permeability of catalyst layer (m^2)	1.0E−13 (assumed based on [48])
Contact angle in GDL and catalyst layer (°)	120
Hydrogen diffusivity ($m^2\,s^{-1}$)	0.915E−4 [62]
Oxygen diffusivity ($m^2\,s^{-1}$)	3.0E−5 [62]
Water vapor diffusivity ($m^2\,s^{-1}$)	3.0E−5 [62]
Electro-osmotic drag coefficient	1.0 [63]
Transfer coefficient at anode, $\alpha_a = \alpha_c$	1.0 [20]
Anode reference exchange current density ($A\,m^{-3}$)	1.5E9 (assumed)
Transfer coefficient at cathode, $\alpha_a = \alpha_c$	1.0 ($V_{cell} < 0.5$ V) [51] 0.5 ($V_{cell} > 0.5$ V)
Cathode reference exchange current density ($A\,m^{-3}$)	1.1E2 ($V_{cell} < 0.5$ V) (fitted) 3.0E5 ($V_{cell} > 0.5$ V)
Entropy change ΔS for $H_2 + \frac{1}{2}O_2 \rightarrow H_2O_{(liq)}$ ($J\,mol^{-1}\,K^{-1}$)	−162.4

using a single-phase model in the membrane is to slightly overestimate the effects of liquid water accumulation in catalyst layers and GDLs on polarization behavior.

2.2. Heat transport model

We also assume that the gas and liquid phases as well as the porous matrix are in local thermal equilibrium. Hence we use a single equation derived by summation of the respective phase heat transport equations to estimate the temperature distribution. The heat generation is modeled using appropriate source terms in different regions of the fuel cell. The model accounts for heat generation due to

1. activation polarization in catalyst layers,
2. ohmic polarization in catalyst layers and the ionic membrane,
3. reversible heat loss,
4. phase change and
5. heat generation due to flow of electric current in the GDLs and at the GDL/bipolar plate interface.

Also, the entire reversible heat loss is assumed to occur in the cathode catalyst layer.

2.3. Electrochemistry

We solve for transport of protons in the catalyst layers and membrane. The solid-phase potential in the catalyst layers is assigned according to the boundary conditions. The effect of electrical contact resistance is also taken into account in the boundary conditions. The electrochemical reactions are modeled by the Butler-Volmer reaction rate expressions [41] which are

modified to include the effect of liquid accumulation on the reaction rates by assuming proportionality to the phase volume fractions.

2.4. Channel flow model

We solve for pressures and component balances in the channels to determine the pressures and concentrations of different species at different distances form the inlet. The pressures and concentrations so determined are then used as boundary conditions for the two-dimensional model used in our work. This allows us to simulate the polarization behavior at different distances form the inlet.

The pressure variation is calculated using the Darcy friction factor law [42] to account for the effect of wall friction. The reactant concentrations are calculated using simple mass balances accounting for the production/consumption of reactants and products [43]. The water produced at the cathode is assumed to mix with the cathode gas stream in the form of water vapor, and phase change of water vapor in the gas channels is neglected. The temperature change of the reactant gases is also neglected. In spite of these simplifications, the above method of calculating the parameters takes into account the effect of reactant flow rates, channel length and active area, which otherwise cannot be accounted for in a two-dimensional model. It is noticed that the parameter values calculated above depend on the current density, which is obtained from the solution of the electrochemistry model. Hence the pressure and concentration boundary conditions are also updated during each iteration of the numerical scheme.

3. Constitutive relations

In order to complete the description of the model presented in the previous section, constitutive relations for various properties are required. The constitutive relations used in this work are given in Table 3. We developed a correlation for the interfacial area density using the existing pore-scale modeling and experimental data [44–46] for different porous media. The correlation is plotted in Fig. 2 along with the experimental and modeling data, and it shows an intermediate shape between the model results. We also correlated the available experimental data [47] for diffusivity of water vapor through the ionic membrane. We use the correlation developed by Gostick et al. [48] for capillary pressure in a GDL. The E-Tek carbon cloth used by Gostick and coworkers for their measurements was almost completely hydrophilic, whereas experiments show that the carbon cloth used in the E-Tek electrode (E-Tek electrode has been used in the experimental study used to validate the model) is hydrophobic [27]. Therefore we correct the capillary pressure obtained by their correlation for contact angle. We also express the equivalent thermal conductivity of the GDL (see Table 1) in terms of the thermal conductivity of a dry GDL to facilitate the use of existing experimental data [49]. We use published correlations for membrane water content at 80 °C [50], ionic conductivity [25] and temperature dependence of cathode reaction rate [51].

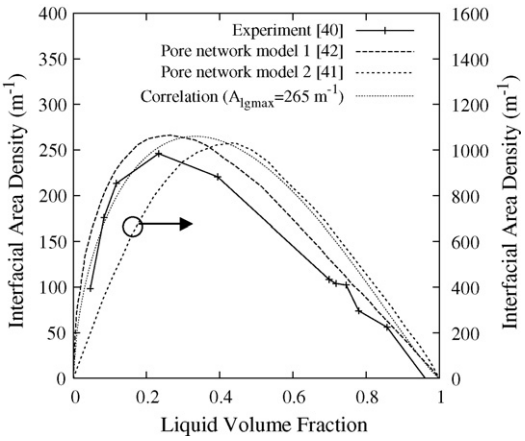

Fig. 2. Variation of interfacial area with liquid volume fraction in a porous medium.

4. Boundary conditions

The boundary conditions required at various interfaces are now described in detail.

4.1. Flow and concentration boundary conditions

The channel pressures as well as the concentrations of reactants and products on the anode and cathode sides are specified as boundary conditions at the GDL/gas channel interfaces. Pressures and concentrations at different distances from the inlet are calculated using the channel flow model described previously. As we use a single-phase model in the ionic membrane, the liquid velocity at the catalyst layer/membrane interface is set to zero.

4.2. Electrochemistry

In the current model the electrochemical equations are solved over the MEA. At the GDL/anode interface, they are

$$\phi_s = U_o - V_{cell} - i_{tot} A R_{a,contact} - i_{tot} A R_{gdl} \quad (1a)$$

$$\nabla \phi_m = 0 \quad (1b)$$

At the GDL/cathode interface, they are

$$\phi_s = i_{tot} A R_{c,contact} + i_{tot} A R_{gdl} \quad (2a)$$

$$\nabla \phi_m = 0 \quad (2b)$$

Again the analysis presented above is simplified and more complicated issues involving the anisotropic electrical conductivity of the GDLs [32,33] have not been addressed. It should also be noted that the above boundary conditions are dependent on the current density. They are also updated during each iteration of the numerical scheme, as in case of the flow boundary conditions. The corresponding heat generation terms due to contact and GDL electrical resistance are also added to the heat equation in the GDLs.

Table 3
Constitutive relations

Expression	Ref.
Capillary pressure: $\alpha_{wp} = \left(1 + \left(\frac{J}{J_c}\right)^n\right)^{-m}$ where $J = \frac{p_{c,air-water}}{\sigma}\left(\frac{K_p}{\varepsilon}\right)^{\frac{1}{2}}$ and $J_c = 0.6982$, $n = 3.465$ and $m = 0.7114$; $p_c = p_{c,air–water}\cos\theta$	[48]
Corrections in property values: $D_g^i = D_{g,o}^i \varepsilon^{1.5}\alpha_g^{3.0}$; $K_{gr} = \alpha_g^{3.0}$, $K_{lr} = \alpha_l^{3.0}$	
Interfacial area density: $A_{lg} = 3.14 A_{lg\,max}\alpha_l^{0.6}\alpha_g^{1.2}$	See Fig. 2
Membrane water content at 80 °C: $\lambda = 0.300 + 10.8a - 16.0a^2 + 14.1a^3$	[50]
Ionic conductivity: $\kappa = 0.5(f - 0.06)^{1.5}\exp\left[\frac{15{,}000}{R}\left(\frac{1}{310.0} - \frac{1}{T}\right)\right]$ where $f = \frac{\lambda V_0}{V_m + \lambda V_0}$ and $V_m = \frac{EW}{\rho_m}$	[25]
Vapor diffusivity in the membrane: $D_{g,mem}^{H_2O} = (3.18633 \times 10^{-10})a - 5.23356 \times 10^{-11}$	
Temperature dependence of exchange current density: $i_{oc}^{ref}(T) = i_{oc,o}^{ref}(353\,K)\exp\left[-\frac{\Delta E}{R}\left(\frac{1}{T} - \frac{1}{353.15}\right)\right]$	[51]
Equivalent thermal conductivity: The expression for $\mathbf{k}_{eq}$ given in Table 1 can be simplified as, $\mathbf{k}_{eq} = \mathbf{k}_{dry} + \varepsilon\alpha_l(\mathbf{k}_l - \mathbf{k}_g)$ where $\mathbf{k}_{dry} = \begin{bmatrix} k_{xx} & 0 \\ 0 & k_{yy} \end{bmatrix}$ and k_{xx} and k_{yy} are experimentally measured through-plane and in-plane thermal conductivities. The liquid and gas thermal conductivities are isotropic.	[49]

4.3. Heat transfer

The heat transfer at the GDL/gas channel interface, current collector/gas channel interface and the current collector/coolant channel interface occurs due to convection. Characteristic *Re* numbers for flow in the gas and coolant channels are low and in the laminar range. Further, the hydrodynamic and thermal entry lengths are relatively short compared to channel lengths. Hence, the convective heat transfer coefficients for the gas and coolant channels are calculated using the following relation applicable for laminar fully developed flows in square channels [52].

$$Nu = \frac{h d_{hyd}}{k_f} = 2.98 \tag{3.1}$$

where

$$d_{hyd} = \frac{4A_{cross}}{P} \tag{3.2}$$

Additionally, the channel boundaries are at nearly a uniform temperature. The effect of a variable temperature along the GDL boundary on the overall heat transfer coefficient is neglected. The gas and coolant temperatures were assumed to be at 353 K (cell operating temperature).

Also, as the two-dimensional domain used in our work is a symmetrical section, all other boundaries are assumed to obey symmetry boundary conditions.

5. Numerical scheme

The set of two-dimensional conservation equations for species, electrochemistry, fluid flow and heat conduction was solved iteratively over the computational domain shown by dotted lines in Fig. 1. The values of various parameters used for the model are given in Table 2. The heat conduction equation was solved until the relative error in the overall heat balance was $<10^{-3}$, and the flow equations were solved using the SIMPLER scheme [53] until the relative error mass balance was $<10^{-10}$. The iterations continued until convergence criteria for all the equations were simultaneously met. The solution was obtained for successively refined grids and a Cartesian grid of size 31×10 provided a grid independent solution. The polarization curve was obtained using the model, and the cathode reference exchange current density was used as a fitting parameter [41] along with the catalyst layer porosity. Since the porosity of the E-Tek electrode catalyst layer used in the experiment [54] used for validation is not known, the electrode porosity was used as a fitting parameter for the model. Mench et al. [54] humidify the anode stream to a temperature above the fuel cell operating temperature. Since the fuel cell is maintained at a lower temperature than the anode humidification temperature, the excess water vapor in the anode stream will most probably condense near the inlet. It is not possible to predict using our model if the water vapor condenses and is carried forward in the form of droplets in the gas stream or if the water vapor condenses at the anode GDL/gas channel interface and then penetrates the anode GDL. Hence for the purposes of this model we assume the anode

to be fully humidified at the fuel cell temperature and that none of the condensed water penetrates the anode GDL.

The experimental polarization curves at different distances from the inlet [54] along with the model predictions are shown in Fig. 3. It can be seen that even with a two-dimensional model the polarization behavior at different distances from the inlet can be predicted with a good degree of accuracy.

6. Discussion of results

In this work, we study the effects of the anisotropic thermal conductivity of the GDLs, GDL width and the width of the current collector ribs on the polarization behavior at different operating conditions. Fig. 3 shows that the effect of liquid accumulation in the cathode GDL and catalyst layer is more significant at lower voltages. In general, the operating voltage depends on the type of application for which the fuel cell is used. Higher voltages generate lower current densities at higher efficiencies, whereas lower voltages generate higher current densities but at lower efficiencies. We analyze results at three different voltages (0.65, 0.6 and 0.55 V) at which the current densities range from about 50–80% of the maximum current density in Fig. 3. Also, the inlet flows are generally humidified to maintain the ionic conductivity of the ionic membrane. Therefore, we also investigate the polarization behavior at different cathode inlet humidities. Also, for Figs. 4–10, values of the parameters kept constant are given in Table 2.

6.1. Fully humidified cathode inlet

Figs. 4 and 5 show the variations of current density, maximum fuel cell temperature, membrane ionic conductivity and cathode catalyst layer liquid volume fraction near the inlet for different values of in-plane and through-plane thermal conductivities of the GDL. Lower through-plane thermal conductivity leads to higher temperatures. Higher temperatures allow more liquid water to evaporate which reduces the amount of liquid water accumulated in the cathode catalyst layer. Higher temperatures, however, also reduce the water vapor activity and

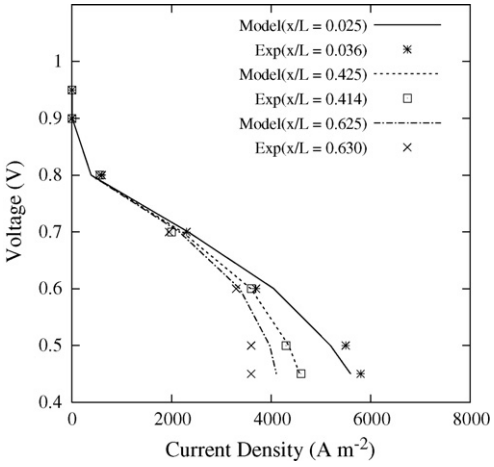

Fig. 3. Comparison of experimental [54] and model polarization results.

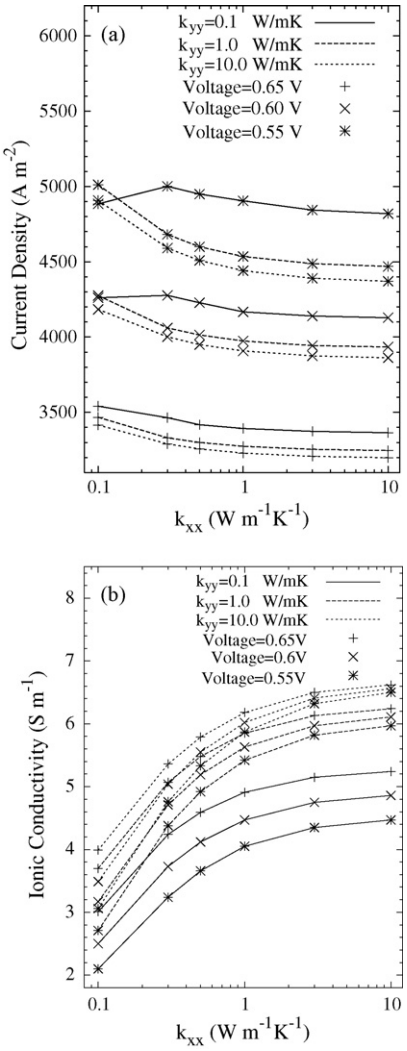

Fig. 4. Variation of (a) current density and (b) ionic conductivity with thermal conductivity of the GDL near the inlet for fully humidified cathode inlet flow.

hence adversely affect the membrane ionic conductivity. Thus increasing the through-plane thermal conductivity of the GDL leads to two competing effects: an increase in the amount of liquid water at the cathode catalyst layer tends to reduce the current density, whereas a higher ionic conductivity of the membrane tends to increase the current density. Since the relative magnitudes of these two competing effects depend on the through-plane thermal conductivity of the GDL, the variation of current density with through-plane thermal conductivity can be expected to show a maximum at a particular value of the through-plane thermal conductivity. The variation of current density with increasing through-plane thermal conductivity (see Fig. 4a) shows a maximum for low in-plane thermal conductivities at lower voltages. At higher in-plane thermal conductivities, however, the current density decreases with increasing through-plane thermal conductivity for all the voltages. Thus, at higher in-plane thermal conductivities, the adverse effect of higher liquid accumulation in the catalyst layer dominates and the current density decreases with increasing through-plane thermal conductivity. At low in-plane thermal conductivities and lower voltages the

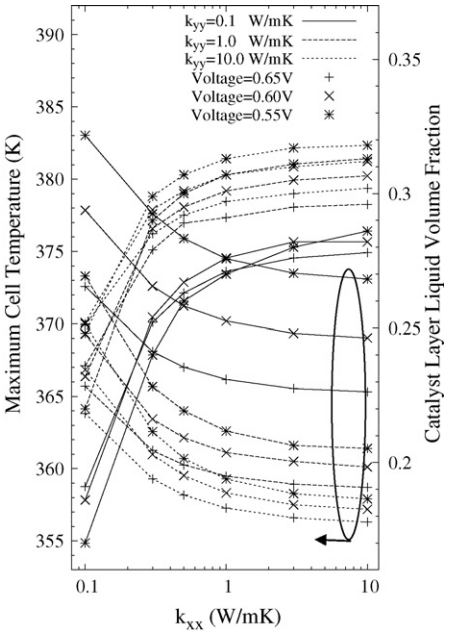

Fig. 5. Variation of maximum fuel cell temperature and catalyst layer liquid volume fraction with thermal conductivity of the GDL near the inlet for fully humidified cathode inlet flow.

temperatures are higher and the membrane ionic conductivities are lower. Hence the variation of current density with increasing through-plane thermal conductivity shows a maximum at lower voltages and lower in-plane thermal conductivities. Lower voltages generate higher current densities which lead to the production of more liquid water and also higher temperatures due to higher heat generation. Hence it is important to determine if the higher temperatures produced at lower voltages are able to

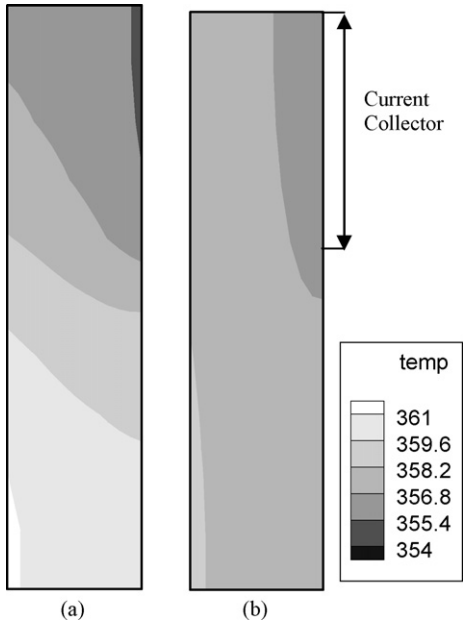

Fig. 6. Comparison of temperature distributions in the cathode GDL for low and high in-plane GDL thermal conductivities for fully humidified cathode inlet flow. (a) $k_{xx} = 1.0\,\mathrm{W\,m^{-1}\,K^{-1}}$ and $k_{yy}/k_{xx} = 1.0$; (b) $k_{xx} = 1.0\,\mathrm{W\,m^{-1}\,K^{-1}}$ and $k_{yy}/k_{xx} = 10$.

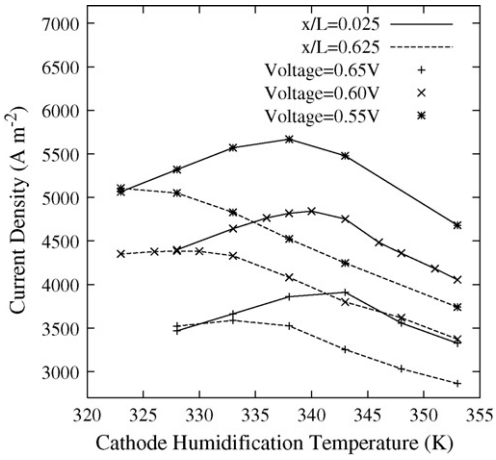

Fig. 7. Variation of current density with cathode humidification temperature at different distances from inlet.

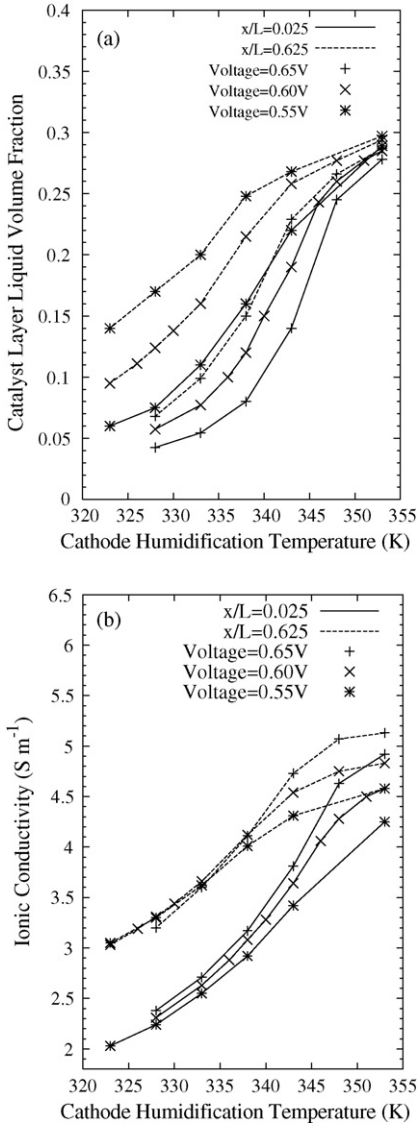

Fig. 8. Variation of (a) catalyst layer liquid volume fraction and (b) ionic conductivity with cathode humidification temperature at different distances from inlet.

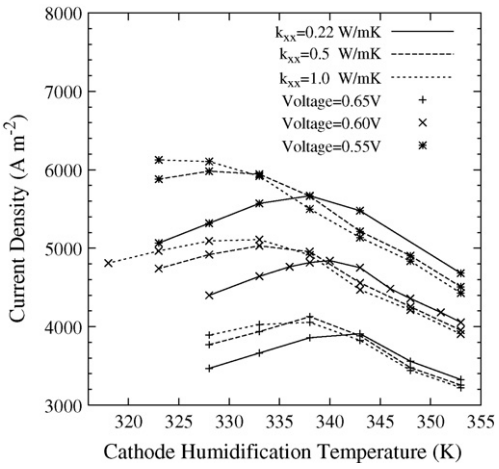

Fig. 9. Variation of current density with cathode humidification temperature near fuel cell inlet for different through-plane thermal conductivities of the GDL.

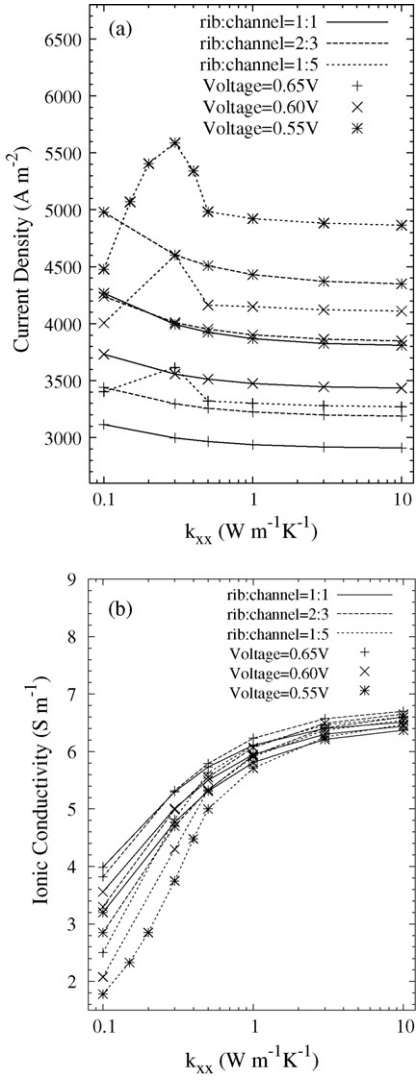

Fig. 10. Variation of (a) current density and (b) ionic conductivity with through-plane thermal conductivity of the GDL for different rib widths near inlet at fully humidified cathode inlet flow condition.

evaporate the higher amount of liquid water produced at lower voltages. Fig. 5 shows that, at lower through-plane thermal conductivities the predicted maximum temperatures are higher for lower voltages. Because of these high temperatures, the liquid water is able to evaporate and liquid accumulation in the cathode catalyst layer is less for lower voltages than that for higher voltages. However, as the through-plane thermal conductivity increases, the temperatures are lowered and the liquid accumulation in the cathode catalyst layer at lower voltages increases to a value above that for higher voltages. Even though higher temperatures reduce liquid accumulation in the catalyst layer and GDL, such high temperatures also tend to adversely affect the long term durability of the ionic membrane [55]. Hence it is desirable to achieve higher current densities without creating excessively high temperatures.

The effects of increasing in-plane thermal conductivity on current density, maximum fuel cell temperature, membrane ionic conductivity and cathode catalyst layer liquid volume fraction are also shown in Figs. 4 and 5. Higher in-plane thermal conductivities lead to lower temperatures. Lower temperatures lead to higher liquid volume fractions in the cathode catalyst layer and also higher ionic conductivity. It can also be noticed that the current density remains almost the same for low through-plane thermal conductivities with increasing in-plane thermal conductivity for all voltages shown in Fig. 4a. As shown in Fig. 6, higher in-plane thermal conductivities create more uniform temperatures than lower in-plane thermal conductivities. It can also be noticed in Fig. 6 that the maximum temperature is lower if the in-plane thermal conductivity of the GDL is high. Higher in-plane thermal conductivities thus reduce the risk of formation of hot spots in the region directly exposed to gas channel and also reduce the possibility of excessively low temperatures in the region directly in contact with the current collector. More uniform temperatures thus reduce the susceptibility of local dry-out of the ionic membrane in the region directly exposed to gas channel and also reduce the possibility of excessive liquid accumulation in the low temperature regions. Thus a combination of high in-plane thermal conductivity and a low through-plane thermal conductivity of the GDL yields higher current densities.

The effects of liquid water accumulation are more severe in regions further away from the inlet due to reduction in reactant concentration and a highly humidified cathode stream created by the product water joining the cathode gas channel. Hence in general, in order to maximize the current density under fully humidified inlet conditions, the through-plane thermal conductivity of the GDL should be as low as possible and the in-plane thermal conductivity should be as high as possible.

6.2. Low humidity cathode inlet

The effects of low humidity operation on current density, ionic conductivity and catalyst layer liquid volume fraction are shown in Figs. 7 and 8. We show the results at two different distances from the inlet. The ionic conductivity and liquid accumulation in the catalyst layer are reduced due to the lower cathode humidity. However, the reduction in liquid accumulation in the cathode catalyst layer has a significant impact on

current density and hence the current density increases with lower humidity. If the inlet cathode humidity is reduced below a certain value, the effect of lower ionic conductivity starts to dominate and the current density decreases. Thus, for low humidity operation, the region near the inlet may experience membrane dehydration while the regions away from the inlet generate higher current densities. Thus, even though a low cathode humidity improves current densities away from the inlet, the adverse effect of membrane dehydration prevents the use of low cathode inlet humidities.

In order to address the problem of membrane dehydration near inlet at low humidities, Dong et al. [56] suggest using a fully humidified anode inlet flow at a temperature above the fuel cell operating temperature. With an aim to develop an alternative methodology to address the problem of membrane dehydration near inlet, we now investigate the effect of GDL thermal conductivities on low humidity operation. Fig. 9 shows the variation of current density near the inlet for different through-plane thermal conductivities at low humidities. Higher through-plane thermal conductivities result in higher current densities at lower cathode humidities. Higher through-plane thermal conductivities in conjunction with high in-plane thermal conductivities (see Table 2) result in lower and more uniform temperatures inside the fuel cell which in turn lead to a higher water vapor activity and hence reduce the risk of membrane dehydration near the inlet. At lower voltages, higher through-plane thermal conductivity leads to higher liquid accumulation in the cathode catalyst layer. Therefore, the maximum current density at a given through-plane thermal conductivity occurs at a lower humidification temperature for lower voltages.

The analysis presented in Section 6.1 shows that high through-plane thermal conductivities promote liquid accumulation in the catalyst layer at fully humidified inlet conditions. The effect of liquid accumulation is more severe in regions away from the inlet because the cathode gas channel humidity increases towards the flow channel exit. Therefore, the current density can be increased if membrane dehydration can be prevented near the inlet without allowing liquid water to accumulate in the region away from the inlet. The current density can thus be increased by constructing a GDL with a high through-plane thermal conductivity near the inlet of the flow channel and progressively, lower through-plane thermal conductivity in regions away from the inlet. The through-plane thermal conductivity of the GDL at any distance from the inlet can be optimized to provide the maximum current density at a given cathode humidity and operating voltage. The GDL can then be constructed to have these optimized thermal conductivities at appropriate distances along the flow channel to maximize the current density at the operating voltage. The through-plane thermal conductivity of the GDL can thus be tailored to reduce the susceptibility of membrane dehydration near inlet and also to reduce the risk of liquid accumulation in the catalyst layer in regions away from the inlet.

6.3. Effect of rib width

The effect of rib width variation on fuel cell operation has been analyzed previously [57–60] from the point of view of reducing the resistance to reactant diffusion and electron transport. In our previous work [36] we used a single-phase model to analyze the effect of variation of rib width on temperature distribution inside a fuel cell. We showed that narrower ribs lead to higher temperatures and using GDLs with highly anisotropic thermal conductivity (higher in-plane thermal conductivity) leads to uniform and lower temperatures. We extend our analysis further in this work.

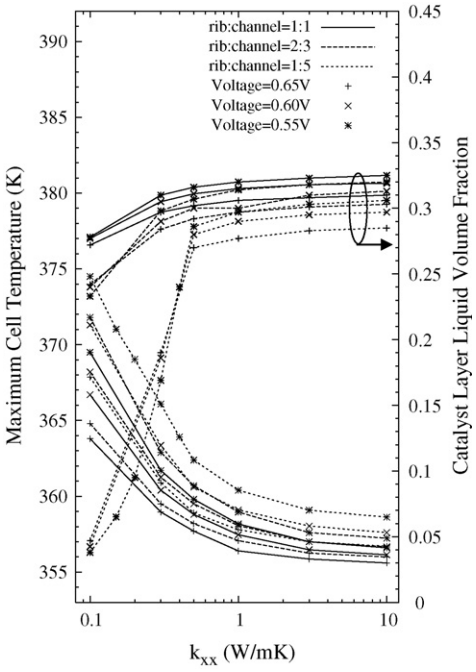

Fig. 11. Variation of maximum fuel cell temperature and catalyst layer liquid volume fraction with through-plane thermal conductivity of the GDL for different rib widths near the inlet at fully humidified cathode inlet flow condition.

Figs. 10 and 11 show the effect of variation of through-plane thermal conductivity on current density, ionic conductivity, maximum fuel cell temperature and cathode catalyst layer liquid accumulation for different rib widths. The results shown in Figs. 10 and 11 are for fully humidified cathode and anode flows near the inlet. Narrower ribs reduce the resistance to diffusion of water vapor from cathode catalyst layer to the gas channel. This reduction in water vapor diffusion resistance lowers the accumulation of liquid water in the cathode catalyst layer. Hence, for the voltages shown in Figs. 10 and 11, smaller rib widths lead to higher current densities. Fig. 11 also shows that the temperatures are higher for narrower ribs for all the considered voltages. Narrower ribs lead to higher temperatures, because higher current densities lead to more heat generation and smaller rib widths reduce the area of heat transfer from the GDL to the coolant channel. Also, the variation of current density with increasing through-plane thermal conductivity shows a maximum in case of small rib widths (rib:channel = 1:5 in Fig. 10). Lower through-plane thermal conductivities lead to higher temperatures which reduce liquid accumulation in the cathode catalyst layer and also reduce the ionic conductivity of the membrane. In addition, as seen from Fig. 11, the accumulation of liquid water in the cathode catalyst layer is reduced for narrower ribs.

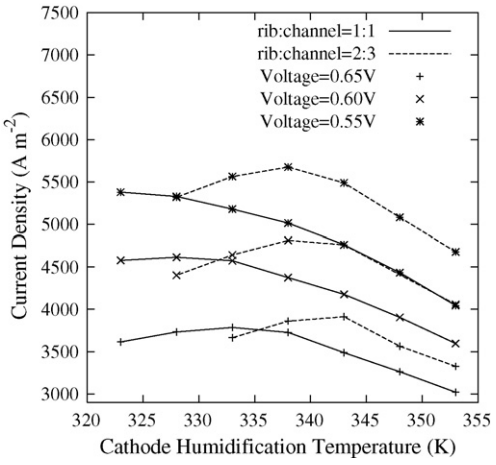

Fig. 12. Variation of current density with cathode humidification temperature near fuel cell inlet for different rib widths.

In case of fuel cells using narrow ribs and GDLs with low through-plane thermal conductivities, the reduced membrane ionic conductivity has a larger negative impact on current density than the positive effect of reduction in cathode catalyst layer liquid accumulation. Therefore, for fuel cells using narrow ribs and operating at fully humidified inlet condition, the through-plane thermal conductivity should be maintained at a higher value in order to maximize the current density near the inlet. In regions further away form the inlet, the humidity of the cathode gas channel flow is higher and lower through-plane thermal conductivities can be used without adversely affecting the current density. Therefore, the methodology to tailor the GDL through-plane thermal conductivity proposed in Section 6.2 can also be used to maximize the current density for fuel cells using narrow ribs and operating at fully humidified inlet conditions. In the present analysis, we have not considered the effect of reducing the rib width on electron transport [58] and also on the structural strength of the current collector plate. The current density of the fuel cell operating at fully humidified inlet conditions is maximum if the current collector rib is as narrow as permitted by the structural strength and electron transport limitations.

Fig. 12 shows the effect of rib width on low humidity operation near the inlet. Narrower ribs generate higher current densities even at lower cathode humidities by reducing the resistance to diffusion of gases through the GDL. However, at cathode humidities lower than an optimum value, wider ribs are able to generate higher current densities. Wider ribs are therefore more effective in reducing the susceptibility of membrane dehydration near the inlet. However, as discussed earlier in this section, narrower ribs are able to generate higher current densities at fully humidified inlet conditions. Hence it would be desirable to use wider ribs near the inlet and narrower ribs in the region away from the inlet in order to maximize the current density at low humidity operating conditions. The width of the ribs can thus be tailored to obtain maximum current density at a given voltage and given cathode inlet humidity.

6.4. Effect of GDL thickness

The effect of reducing GDL thickness on current density is similar to the effect of narrower current collector ribs on current density. Within the computational domain of Fig. 1, a certain fraction of the GDL surface is exposed to the gas channel and the other fraction is directly in contact with the current collector ribs. In the region of GDL directly exposed to the gas channel, smaller GDL thickness reduces the resistance to diffusion of water vapor and reactants through the GDL. However, smaller GDL thickness also increases the diffusion resistance in the region of GDL directly in contact with the current collector ribs. Hence there is an optimum thickness below which the current density reduces for smaller GDL thicknesses [58]. In our previous work [36], we showed that most of the heat generated is transported to the coolant channel through the current collector ribs and a very small fraction of the total heat generated is transported to the gas channel. Smaller GDL thicknesses reduce the area of heat transfer from the high-temperature region (the region of the GDL directly exposed to the gas channel) to the current collector ribs. This reduction in heat transfer area results in higher temperatures in the region directly exposed to the gas channel [36]. In the region of the GDL directly in contact with the current collector, thinner GDL also reduces the average temperature and promotes liquid accumulation in this region. We also showed that, using GDLs with highly anisotropic thermal conductivity leads more uniform temperatures. Thus, in case of thin GDLs, anisotropic thermal conductivity plays a more important role in maintaining uniform temperatures and reducing the risk of liquid accumulation than in case of thicker GDLs [36]. We confirmed the conclusions of our previous work, obtained using a single-phase model, using the present two-phase model.

7. Conclusions

A two-dimensional two-phase model is presented to predict the effect of GDL thermal conductivity on the polarization behavior under different operating conditions. The important conclusions from the study are summarized by:

1. The fuel cell generates high current densities with moderately high temperatures for a low value of through-plane thermal conductivity and a high in-plane thermal conductivity of the GDL.
2. By tailoring the GDL to have high through-plane thermal conductivity near the inlet, membrane dehydration may be avoided for low humidity operating conditions.
3. Similarly, the current density may be maximized at low humidity operating conditions by tailoring the GDL to have high through-plane thermal conductivity near the inlet and progressively decreasing through-plane thermal conductivity at distances farther away from the inlet along the flow channel.
4. Narrower current collector ribs lead to higher current densities for fuel cells using fully humidified cathode inlet flow.
5. Near the inlet, fuel cells with wider ribs produce higher current density than those with narrower ribs if the cathode inlet humidity is below a certain value.

6. The current density can be maximized at lower cathode inlet humidities by using wider ribs in the region near the inlet and narrower ribs in the region away form the inlet.

Acknowledgment

Funding from the National Science Foundation (Grant No. CTS-0226095) is gratefully acknowledged.

References

[1] U. Pasaogullari, C.Y. Wang, J. Electrochem. Soc. 151 (2004) A399.
[2] T.F. Fuller, J. Newman, J. Electrochem. Soc. 140 (1995) 1218.
[3] T.V. Nguyen, R.E. White, J. Electrochem. Soc. 140 (1993) 2178.
[4] J.J. Baschuk, X. Li, J. Power Sources 86 (2000) 181.
[5] U. Sukkee, C.Y. Wang, K.S. Chen, J. Electrochem. Soc. 147 (2000) 4485.
[6] V. Gurau, H. Liu, S. Kakac, AICHE J. 44 (1998) 2410.
[7] H. Meng, C.Y. Wang, J. Electrochem. Soc. 152 (2005) A1733.
[8] J.B. Stockie, Proceedings of IMECE'02, 2002 ASME International Mechanical Engineering Congress and Exposition, vol. 7, New Orleans, Louisiana, USA, HTD, November 17–22, 2002, p. 393.
[9] T. Berning, N. Djilali, J. Electrochem. Soc. 150 (2003) A1589.
[10] Z.H. Wang, C.Y. Wang, K.S. Chen, J. Power Sources 94 (2001) 40.
[11] D. Natarajan, T.V. Nguyen, J. Electrochem. Soc. 148 (2001) A1324.
[12] M. Hu, A. Gu, M. Wang, X. Zhu, L. Yu, Energy Convers. Manage. 45 (2004) 1861.
[13] M. Hu, X. Zhu, M. Wang, A. Gu, L. Yu, Energy Convers. Manage. 45 (2004) 1883.
[14] S. Mazumder, J.V. Cole, J. Electrochem. Soc. 150 (2003) A1510.
[15] H. Sun, H. Liu, L. Guo, J. Power Sources 143 (2005) 125.
[16] E. Birgersson, M. Noponen, M. Vynnycky, J. Electrochem. Soc. 152 (2005) A1021.
[17] J.J. Baschuk, X. Li, J. Power Sources 142 (2004) 134.
[18] S. Shimpalee, S. Greenway, D. Spuckler, J.W. Van Zee, J. Power Sources 135 (2004) 79.
[19] H. Meng, C.Y. Wang, Fuel Cells 5 (2005) 455.
[20] H. Meng, J. Power Sources 168 (2007) 218.
[21] C.Y. Wang, P. Cheng, Adv. Heat Transfer 30 (1997) 93.
[22] C.Y. Wang, P. Cheng, Int. J. Heat Mass Transfer 39 (1996) 3607.
[23] H. Meng, J. Power Sources 162 (2006) 426.
[24] A.Z. Weber, J. Newman, J. Electrochem. Soc. 150 (2003) A1008.
[25] A.Z. Weber, J. Newman, J. Electrochem. Soc. 151 (2004) A311.
[26] H. Ju, H. Meng, C.Y. Wang, Int. J. Heat Mass Transfer 48 (2005) 1303.
[27] J. Benziger, J. Nehlsen, D. Blackwell, T. Brennan, J. Itescu, J. Membrane Sci. 261 (2005) 98.
[28] K. Kurabayashi, Int. J. Thermophys. 12 (2001) 277.
[29] D. Hansen, G.A. Bernier, Poly. Eng. Sci. 12 (1972) 204.
[30] D.T. Morelli, J. Heremans, M. Sakomoto, C. Uher, Phys. Rev. Lett. 57 (1986) 869.
[31] K. Kurabayashi, M. Asheghi, M. Touzelbaev, K.E. Goodson, IEEE J. Microelectromech. Sys. 8 (1999) 180.
[32] Toray Industries Inc., GDL specification sheet.
[33] M. Mathias, J. Roth, J. Fleming, W. Lehnert, in: W. Vielstich, H.A. Gasteiger, A. Lamm (Eds.), Handbook of Fuel Cells—Fundamentals, Technology and Applications. Vol. 3: Fuel Cell Technology and Applications, John-Wiley and Sons Ltd., Chichester, England, 2003, p. 517.
[34] U. Pasaogullari, P.P. Mukherjee, C.Y. Wang, K.S. Chen, ECS Trans. 3 (2006) 1239.
[35] J.G. Pharoah, K. Karan, W. Sun, J. Power Sources 161 (2006) 214.
[36] C.J. Bapat, S.T. Thynell, J. Heat Transfer 129 (2007) 1109.
[37] M. Ishii, Thermo-Fluid Dynamic Theory of Two-Phase Flow, Eyrolles, Paris, 1975.
[38] D.A. Drew, S.L. Passman, Theory of Multicomponent Fluids, Springer-Verlag, New York, NY, 1999.
[39] M. Hassanizadeh, W.G. Gray, Adv. Water Resour. 2 (1979) 131.
[40] M. Hassanizadeh, W.G. Gray, Adv. Water Resour. 2 (1979) 191.
[41] D.M. Bernardi, M.W. Verbrugge, J. Electrochem. Soc. 139 (1992) 2477.
[42] R.W. Fox, A.T. McDonald, Introduction to Fluid Mechanics, John-Wiley and Sons, New York, NY, 2001.
[43] A.Z. Weber, J. Newman, J. Electrochem. Soc. 151 (2004) A326.
[44] K.A. Culligan, D. Wildenschild, B.S.B. Christensen, W.G. Gray, M.L. Rivers, A.F.B. Tompson, Water Resour. Res. 40 (2004) W12413.
[45] R.J. Held, M.A. Celia, Adv. Water Resour. 24 (2001) 325.
[46] P.C. Reeves, M.A. Celia, Water Resour. Res. 32 (1996) 2345.
[47] D. Rivin, C.E. Kendrick, P.W. Gibson, N.S. Schneider, Polymer 42 (2001) 623.
[48] J.T. Gostick, M.W. Fowler, M.A. Ioannidis, M.D. Pritzker, Y.M. Volfkovich, A. Sakars, J. Power Sources 156 (2006) 375.
[49] M. Khandelwal, M.M. Mench, J. Power Sources 161 (2006) 1106.
[50] J.T. Hinatsu, M. Mizuhata, H. Takenaka, J. Electrochem. Soc. 141 (1994) 1493.
[51] A. Parthasarathy, S. Srinivasan, J.A. Appleby, J. Electrochem. Soc. 139 (1992) 2530.
[52] R.K. Shah, A.L. London, Laminar Flow Forced Convection in Ducts, Academic Press, New York, 1978.
[53] S.V. Patankar, Numerical Heat Transfer and Fluid Flow, Hemisphere, Washington, DC, 1980.
[54] M.M. Mench, C.Y. Wang, M. Ishikawa, J. Electrochem. Soc. 150 (2003) A1052.
[55] J. Zhang, Z. Xie, J. Zhang, Y. Tang, C. Song, T. Navessin, Z. Shi, D. Song, H. Wang, D.P. Wilkinson, Z.S. Liu, S. Holdcroft, J. Power Sources 160 (2006) 872.
[56] Q. Dong, M.M. Mench, S. Cleghorn, U. Beuscher, J. Electrochem. Soc. 152 (2005) A2114.
[57] K.T. Jeng, S.F. Lee, G.F. Tsai, C.H. Wang, J. Power Sources 138 (2004) 41.
[58] S.M. Senn, D. Poulikakos, J. Heat Transfer 127 (2005) 1245.
[59] T. Berning, N. Djilali, J. Power Sources 124 (2003) 440.
[60] S.A. Grigoriev, A.A. Kalinnikov, V.N. Fateev, A.A. Wragg, J. Appl. Electrochem. 36 (2006) 191.
[61] A. Hollinger, Contact Resistance Measurements of Gas-diffusion layers and Membrane for Fuel Cell Applications, Senior Honors Thesis, Department of Engineering Science and Mechanics, The Pennsylvania State University, University Park, PA, 2006.
[62] E.L. Cussler, Multicomponent Diffusion, Elsevier Scientific Pub. Co., Amsterdam, New York, 1976.
[63] T.A. Zawodzinski, J. Dawy, J. Valerio, S. Gottesfeld, Electrochim. Acta 40 (1995) 297.